Applied Catalysis A, General 661 (2023) 119243

Contents lists available at ScienceDirect

Applied Catalysis A, General

journal homepage: www.elsevier.com/locate/apcata

1-Butanol dehydration and oxidation over vanadium phosphate catalysts

Francesco Puzzo [a], Noemi Capece [a], Laura Setti [a], Giulia Pavarelli [a], Jacopo De Maron [a,b], Tommaso Tabanelli [a,b], Fabrizio Cavani [a,b,*]

[a] Dipartimento di Chimica Industriale "Toso Montanari", Alma Mater Studiorum Università di Bologna, Viale Risorgimento 4, 40136 Bologna, Italy
[b] Center for Chemical Catalysis C3, Alma Mater Studiorum Università di Bologna, Italy

ARTICLE INFO

Keywords:
1-butanol
Butenes
Maleic anhydride
Selective oxidation
Vanadyl pyrophosphate
Vanadium phosphate

ABSTRACT

The transformation of 1-butanol into either butenes or maleic anhydride was carried out both with and without oxygen, using V/P/O catalysts. With vanadyl pyrophosphate prepared by coprecipitation, at temperature lower than 240 °C and without oxygen, selectivity to butenes was higher than 90%, but a slow deactivation took place. At temperature higher than 300 °C and in the presence of air, maleic and phthalic anhydrides were the prevailing products, with selectivity of 60% and 14%, respectively. Catalytic performance was affected by crystallinity and acidity. α_I-$VOPO_4$ showed a poor performance in the absence of air, with a quick deactivation due to coke accumulation; but it displayed an excellent selectivity to butenes (close to 98%) at temperatures lower than 320 °C in the presence of air, with stable performance. At temperature higher than 360 °C, α_I-$VOPO_4$ was reduced to vanadyl pyrophosphate and catalyzed the direct oxidation of 1-butanol into maleic anhydride, but with 35% selectivity.

1. Introduction

The catalytic transformation of bio-alcohols into chemicals may represent an alternative to current industrial chemical processes based on fossil sources; for example, the synthesis of alkenes via alcohols dehydration might compete with steam-cracking or FCC of oil fractions [1–4]. Ethanol and 1-butanol, which are currently the most produced bio-alcohols worldwide, represent the most investigated reactants [5,6].

The dehydration of ethanol to ethylene is commercially available; the reaction is carried out at 300–350 °C and 5 bar pressure [7]. There are many efficient catalysts for ethanol dehydration, such as supported phosphoric acid, alumina, silica-alumina, zeolites (H-ZSM5) and SAPO-34 [8–14].

Butanols (mainly 1-butanol, but also 2-butanol, isobutanol and *tert*-butanol) dehydration has been investigated by several research groups [15–35]. Millet and co-workers deeply investigated the gas-phase dehydration of 1-butanol with rare earth phosphates, which proved to be very efficient catalysts for the dehydration of 1-butanol to 2-butene, and for the dehydration of alcohols mixtures as well [15–17]. It was reported that the reaction involves the moderately strong Brønsted and Lewis acid sites on catalysts surface. Lanthanum orthophosphate displayed the best performance [16]. Crystallinity, surface area, surface composition and acid–base properties of La/P/O differed according to the preparation method used, but the most important parameter influencing catalytic properties was surface composition which had a direct effect on surface acidity. Brønsted acid sites appeared as the most efficient, associated with the presence of an excess of phosphorus; the mechanism for 1-butanol dehydration is an E1-type elimination [15].

Zeolites have also been investigated as catalysts for 1-butanol dehydration. For example, Verberckmoes and co-workers [18–21] studied different zeolites and alumina catalysts, comparing the reactivity of 1-butanol with other alcohols (isobutanol, ethanol), also by means of microkinetics simulation, and investigating on the effect of the zeolite Si/Al ratio. Marin and co-workers [23–26] reported that the consecutive scheme of 1-butanol condensation to the ether followed by ether decomposition shows lower energy barriers as compared to the direct dehydration of 1-butanol. In the large pore H-FAU, instead, the weaker dispersive stabilization of the dimer makes the butene formation by monomolecular direct dehydration via a concerted anti elimination compete with dibutyl ether formation. With some zeolite types, the direct transformation of 1-butanol into isobutene is also possible, as demonstrated by Chadwick et al. [27]. The role of the different acid sites in ZSM-5 was also investigated by Zhao et al. [28].

Other catalysts investigated for 1-butanol dehydration include

* Corresponding author at: Dipartimento di Chimica Industriale "Toso Montanari", Alma Mater Studiorum Università di Bologna, Viale Risorgimento 4, 40136 Bologna, Italy.
E-mail address: fabrizio.cavani@unibo.it (F. Cavani).

https://doi.org/10.1016/j.apcata.2023.119243
Received 11 December 2022; Received in revised form 24 April 2023; Accepted 30 April 2023
Available online 2 May 2023
0926-860X/© 2023 The Authors. Published by Elsevier B.V. This is an open access article under the CC BY license (http://creativecommons.org/licenses/by/4.0/).

supported Keggin-type polyoxometalates [29,30], WO_3/ZrO_2 [31], Zn-Mn-Co modified γ-Al_2O_3 [32], anatase modified with a phosphonic acid monolayer [33], ammonium Keggin polyoxometalate salts [34], and phosphate modified carbon nanotubes [35].

2-Butanol dehydration has also been investigated by several authors, using various catalyst types: carbon-based catalysts also containing phosphate groups [36], alumina [37], and WO_x-ZrO_2 [38–40].

Ferrierites were found to catalyse isobutanol dehydration to linear butenes [41,42].

Driven by the excellent results reported in literature for the dehydration on metal phosphates by Nguyen et al. [15–17], it was decided to study the reactivity of vanadium phosphates (V/P/O), more specifically, of vanadyl pyrophosphate ($(VO)_2P_2O_7$), the industrial catalyst for the oxidation of *n*-butane to maleic anhydride (MA) [43], and of vanadium phosphate ($VOPO_4$). We previously reported that vanadyl pyrophosphate is active and selective also for the direct transformation of 1-butanol, obtained from bio-based sources, into MA [44]. The first step of the mechanism is the dehydration of 1-butanol into 2-butenes and 1-butene, the quantity of isomers corresponding to the equilibrium one; in the presence of molecular oxygen, the olefins are then transformed into MA. Therefore, it may be expected that in the absence of molecular oxygen the catalyst could be selective in olefins formation from 1-butanol. Moreover, vanadyl pyrophosphate is known to exhibit both redox and acid properties, behaving as a bifunctional catalyst, able to perform acid-catalyzed reactions both in the gas and in the liquid-phase [45–66].

In this paper, we exploit the acid and redox properties of V/P/O catalysts to control the transformation of 1-butanol into either olefins or MA, by means of a proper tuning of reaction conditions, both in the presence and in the absence of air, and by studying the transformations of catalysts occurring during reaction.

2. Experimental

2.1. Catalyst preparation

1. DuPont Vanadyl pyrophosphate (VPP-1)

   The VPP-1 catalyst was made of vanadyl pyrophosphate delivered by DuPont, used in the oxidation of *n*-butane into MA in a circulating-fluid-bed reactor. Details concerning the characteristics of the catalysts are reported in the literature [67].
2. Vanadyl pyrophosphate, prepared by organic medium synthesis (VPP-2)

   The VPP-2 catalyst was prepared by means of the "organic method", according to the procedure reported in literature [48]. $(VO)HPO_4 0.5H_2O$, precursor of vanadyl pyrophosphate, was synthesized by suspending in a stirred three necked round bottom flask the desired amounts of V_2O_5 (99% Sigma Aldrich) and H_3PO_4 (98% Sigma Aldrich) in isobutanol (99% Sigma Aldrich) in order to have a P/V molar ratio equal to 1.1. The mixture was heated at reflux temperature (120 °C) for 6 h. The colour varied from dark orange of V_2O_5, to an intense light blue, which is characteristic of $(VO)HPO_4 0.5H_2O$. After filtration, the obtained precipitate was dried in static air for 12 h at 120 °C, and then thermally treated first in air and later in nitrogen.
3. Vanadium phosphate (VPD)

   $VOPO_4 2H_2O$ (VPD) was prepared by suspending the desired amounts of V_2O_5 (99% Sigma Aldrich) and H_3PO_4 (85% Sigma Aldrich) in water. Phosphoric acid was added in excess (P/V= 4), since in a stoichiometric amount, it does not permit the complete dissolution of V_2O_5 and leads to incomplete conversion of vanadium pentoxide. The mixture was heated at reflux temperature (100 °C) for 17 h, under vigorous stirring: the colour changed from dark orange of V_2O_5 to bright yellow, indicating the formation of $VOPO_4 2H_2O$. The mixture was left for one day at ambient temperature, and the solid obtained was recovered by filtration and dried for few hours at 100 °C. Thermal treatment of the catalyst was performed directly inside the laboratory-scale reactor from room temperature up to 440 °C, followed by an isothermal step at 440 °C for 24 h.

The regeneration of used, deactivated catalysts was carried out according to the following procedure: increase of temperature from room up to 440 °C under flow of air (heating rate: 100 °C/hour; air flow: 60 mL/min); then, isothermal step at 440 °C for 12 h, under flow of air.

2.2. Laboratory-scale plant tests

Catalytic tests were carried out in a continuous-flow, fixed bed, quartz reactor. The system permits variation of different reaction parameters: feed composition, contact time, and temperature.

Typical reaction conditions were the following: 1 g of catalyst shaped in particles (size 0.5–1.0 mm); feed composition 0.1–1.0 mol% 1-butanol in air (details in figures captions); temperature range: from 200 °C until 440 °C maximum (higher temperatures lead to irreversible structural or morphology changes of the V/P/O catalysts). In experiments carried out with temperature increase, the catalyst used was the same at all temperatures.

1-Butanol was continuously fed using a KDS100 pump, inside a stainless-steel line heated at 160 °C, in order to obtain an instant vaporisation and a good mixing with the gas stream (air of He). The reactants and products were analysed using a Varian CP-3380 gas chromatograph, equipped with the following columns and detectors:

- Semicapillar CPSil-5CB column (30 m length; i.d. 0.53 mm; stationary phase for MA, by-products (phthalic anhydride, acetic acid, acrylic acid, and other light compounds, e.g., butenes), and 1-butanol. The detector is a FID.
- Packed Carbosieve SII column (2 m length, stationary phase of active carbons having dimensions of 80-100 mesh). In this column, CO, CO_2, H_2O, O_2, and N_2 are separated and detected by a TCD.

2.3. Catalyst characterisation

The characterisation of catalysts was performed using XRD, BET, TPSR and Raman techniques.

The X-ray powder diffraction (XRD) measurements were carried out using a Philips PW 1710 apparatus, with Cu Kα ($\lambda = 1.5406$ Å) radiation in the range of $5\ ^\circ < 2\theta < 60\ ^\circ$, with steps of 0.05 grade, and signal acquisition for 3 s in each step. X-ray diffraction lines attribution was done by the Bragg law: $2d \text{ sen } \theta = n\lambda$ and by comparing the results obtained with those reported in literature.

The specific surface area was determined by N_2 adsorption at − 196 °C (the boiling T of nitrogen), with a Sorpty 1750 Instrument (Carlo Erba). The sample was heated at 150 °C under vacuum, to eliminate water and other molecules eventually adsorbed on the surface. After this pre-treatment, the sample temperature was maintained at − 196 °C in a liquid nitrogen bath, while gaseous N_2 was adsorbed on the surface. Using the BET equation, the volume of monolayer and finally the sample surface area could be calculated.

Temperature programmed surface reaction (TPSR) experiments were carried out with methanol as the probe molecule, using the Autochem II of Micromeritcs associated to a mass spectrum detector MKS Cirrus. The calcined sample was subjected to an initial pre-treatment, by heating at 300 °C under He, in order to clean the surface from the adsorbed molecules. The pre-treatment did not modify catalyst features; in fact, V/P/O catalysts self-reduce spontaneously under inert atmosphere (e.g., in N_2 or He) only for temperatures higher than 430–450 °C, as confirmed by the absence of the O_2 signal during preliminary TPD experiments. Molecular oxygen is released when temperatures higher than 430–450 °C are used, with concomitant reduction of V^{5+} species, if present in the calcined sample.

The adsorption was carried out at 100 °C by pulsing methanol vapours (0.0414 mol%) in the He flow, which was repeated 50 times, for saturating the surface with the probe molecule. Desorption was realized by feeding He and heating the sample at 5 °C/min from 100 °C until 550 °C and the isotherm at that temperature for 30 min. A part of the outlet gases was sent to the mass spectrum detector.

Raman analyses were carried out using a Renishaw Raman System RM1000 instrument, equipped with a Leica DLML confocal microscope, with 5x, 20x, and 50x objectives, video camera, CCD detector, and laser source Argon ion (514 nm) with power 25 mW. The maximum spatial resolution was 0.5 μm, and the spectral resolution was 1 cm^{-1}. For each sample, a wide number of spectra were collected by changing the focus of the laser beam. The parameters of spectrum acquisition were selected as follows: 5 accumulations, 10 s, 25% of laser power to prevent sample damage, and 50x objective.

In-situ Raman experiment analyses were performed using a commercial Raman cell (Linkam Instruments TS1500). Approximately 5–10 mg of the sample was used for the analysis. The air flow, fed from the start of the experiment, was about 10 mL/min. Spectra were recorded at room temperature, while the temperature (heating rate of 100 °C/min) was increased up to the desired value during the isotherm period. The laser power used was 25%, which permits good spectrum acquisition without damaging the sample; the other acquisition parameters were as follows: 10 accumulations, 10 s each; 20x objective.

3. Results and discussion

3.1. Characterisation of the fresh calcined catalysts

The catalysts tested in the dehydration and oxidation of 1-butanol were characterized before reaction by Raman spectroscopy and X-ray Diffraction (Fig. 1a and Fig. 1b, respectively). Several Raman spectra were recorded for each sample, by changing the laser beam position.

The Raman spectra of fresh VPP-1 are shown in Fig. 1 (top, a), presenting the characteristic bands of vanadyl pyrophosphate, at 1185, 1135 and 924 cm^{-1} [46,48,67]. The X-ray diffraction pattern of the fresh VPP-1 catalyst (Fig. 1, top, b) confirms the presence of $(VO)_2P_2O_7$. The surface area of this sample was 40 m^2/g.

Regarding the VPP-2 catalyst, Raman spectra (Fig. 1, middle, a) show spectral features of the vanadyl pyrophosphate, as also confirmed by the

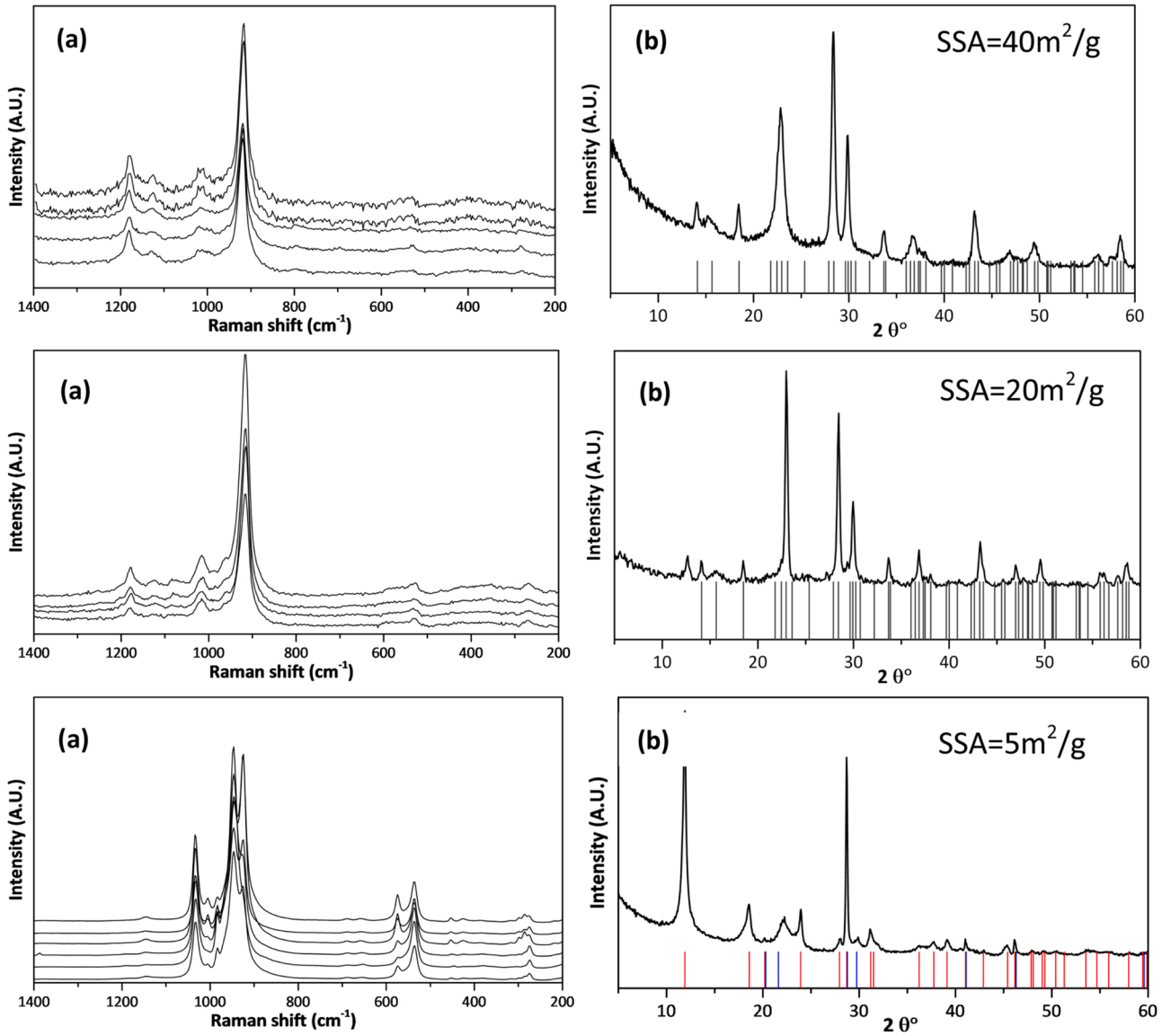

Fig. 1. Raman spectra (a) and XRD patterns (b) of VPP-1 (top), VPP-2 (middle), VPD (bottom). Regarding the XRD, the position of the pattern for the few reference crystal phases is also shown: $(VO)_2P_2O_7$ (black lines), $VOPO_4 2H_2O$ (red lines) and α_1-$VOPO_4$ (blue lines).

XRD pattern (Fig. 1, middle, b). The surface area of this sample was 20 m^2/g.

VPP-2 was more crystalline than VPP-1, as shown by the narrower diffraction lines attributable to vanadyl pyrophosphate. The former sample also displayed a lower surface area, a difference which is in line with the different degree of samples crystallinity.

Raman spectra of the VPD sample, presented in Fig. 1 (bottom, a) show bands attributable to $VOPO_42H_2O$ (at 1039, 988, 952, and 540 cm^{-1}) and α_1-$VOPO_4$ (at 1032, 928, 575 and 540 cm^{-1}) [68]. However, the relative intensity of the bands differed depending on the position of the laser beam, which points out for a non-homogeneous distribution of the two compounds in the catalyst. The XRD pattern reported in Fig. 1 (bottom, b) shows the presence of $VOPO_42H_2O$ and, in minor amount, of α_1-$VOPO_4$. Moreover, this catalyst presents the lower specific surface area of 5 m^2/g, compared to the vanadyl pyrophosphate samples.

The calcination process of the VPD catalyst was also investigated, by monitoring the transformations occurring during the thermal treatment by means of in-situ Raman spectroscopy; spectra are shown in Fig. S1. It was shown that the dehydration of $VOPO_42H_2O$ into α_1-$VOPO_4$ already occurred at below 100 °C.

3.2. *The reactivity of vanadyl pyrophosphate in the oxidation of 1-butanol to MA*

The reactivity of VPP-1 and VPP-2 catalysts was compared; as detailed above, the main difference between the two catalysts was the value of surface area.

Fig. 2 shows the effect of temperature on VPP-1 catalytic performance, with a feed consisting of 0.4 mol.% 1-butanol in air, and W/F= 1.3 $g_{cat}s/mL$. Complete 1-butanol conversion was shown at 200 °C. Noteworthy, also under oxidizing conditions, high yields of butenes, 76% and 15% of 1-butene and 2-butenes, respectively, were obtained by working at temperatures lower than 220 °C with a C balance close to 90%. The molar ratio between 2-butenes and 1-butene was slightly lower than the equilibrium one, 5.0 vs 6.1 [69]. Interestingly, the condensation product, *n*-butyl ether (NBE), was produced with yield lower than 1%. When the temperature was raised up to above 260 °C, 2-butenes showed a higher rate of depletion compared to 1-butene, suggesting that oxidation is quicker than isomerization, and that

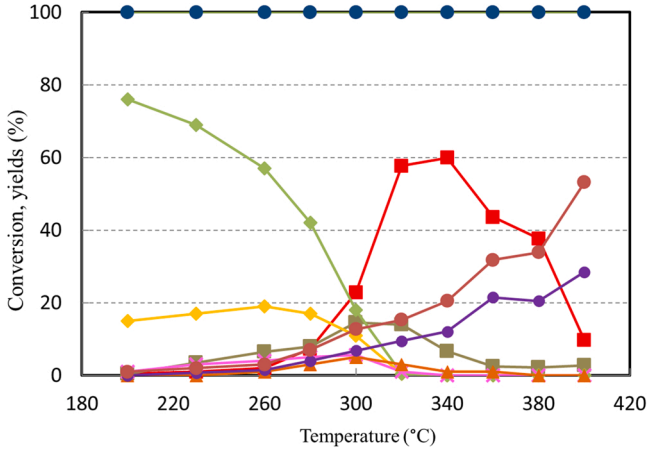

Fig. 2. Temperature effect on the catalytic behaviour of VPP-1 in 1-butanol oxidation. Feed 0.4% mol 1-butanol in air. W/F 1.3 g_{cat} s/mL. Symbols: 1-butanol conversion (●), 1-butene (◆), 2-butenes (◆), maleic anhydride (■); phthalic anhydride (■); acrylic acid + acetic acid (▲); CO (●), CO_2 (●), lights (✕).

oxidation of 2-butenes is quicker than that of 1-butene. Main oxygenated products were MA, phthalic anhydride (PA), acetic acid and acrylic acid (reported as "Sum acids"), lights (mainly formaldehyde), CO and CO_2. In this temperature range, C balance was close to 100%. Hypothesis about the mechanism for PA formation were discussed in previous works [44, 70].

The highest PA yield of 15% was achieved at 300–320 °C, whereas best yield to MA, close to 60%, was shown in the range 320–340 °C. A further increase of the reaction temperature led to a rapid decline of both MA and PA yields, due to the preferred oxidation of intermediates and products to CO and CO_2. In a previous paper, the reactivity of the same catalyst at higher 1-butanol concentration (1.0% in air) was shown [44] (for the sake of an easier comparison, the same figure is reported in the SI, Fig. S2); in that case, maximum yield to MA was 39% only.

Conversion of 1-butanol was complete over the entire range of temperature investigated. In fact, the alcohol is very reactive, and dehydrates into butenes, the only primary products, already at 150 °C; however, higher temperatures are required to transform butenes into oxidised compounds. Experiments carried out at 340 °C in function of contact time with VPP-1 were reported in a previous work [44]; it was shown that intermediates in the oxidation of butenes were crotonaldehyde, furan and maleic acid. Moreover, it was also shown that at 340 °C MA and PA are stable compounds, which do not undergo consecutive combustion, even at total reactant conversion.

Fig. 3 summarizes the effect of 1-butanol concentration on the catalytic performance of VPP-1. In all catalytic tests, complete conversion was achieved. It is shown that an increase of the alcohol content in the feed had a relevant effect on the distribution of products. In particular: (a) the temperature at which the intermediately formed olefins were oxidised into MA and PA was shifted towards higher temperatures (from 320° to 360°C); (b) the highest yield of both PA and MA considerably decreased; MA dropped from 60% down to 39% and 18%, at the 0.4, 1.0 and 2.0 mol% of 1-butanol in feed, respectively.

The experiments shown in Fig. 3 confirm the well-known drawback of the VPP catalyst, i.e., the limited number of surface sites available, hence the easy occurrence of saturation phenomena, especially when reactants which develop strong interaction with the catalyst are used, as in the case of 1-butanol [44,46]. This limitation derives from the low number of V^{5+} sites which develop under reaction conditions at the surface of the vanadyl pyrophosphate [46,48].

Regarding the effect of inlet oxygen molar fraction on catalytic behavior, it was reported in a previous paper [44]. It was shown that an increase in the oxygen content led to an increase in both MA and PA selectivity, whereas there was almost no effect on selectivity to light acids. Selectivity to CO and CO_2 increased slightly in the O_2 molar fraction range 0.04–0.10 and then decreased until the O_2 molar fraction of 0.20. Under the latter conditions, the highest selectivity to MA and PA was recorded.

Because of the surface coverage and saturation by the alcohol and by the intermediately formed olefins [44], a phenomenon which becomes more relevant when higher 1-butanol concentrations are used, the V ability to provide active V^{5+} sites for the transformation of the olefins into MA and PA was considerably decreased. Therefore, higher temperatures were needed for increasing 1-butanol inlet molar fraction, to facilitate desorption of intermediates and products and make more V sites available for the generation of active, oxidising species and for the oxidative steps to occur.

This phenomenon was even more evident with catalyst VPP-2, characterised by a lower surface area than VPP-1. Fig. 4 reports the effect of temperature on catalytic performance, at 1.0 mol% 1-butanol in feed, that is, the same conditions used for VPP-1 and reported in [44] (see Fig. S2). With VPP-2 the best MA yield, achieved at 400 °C, was 50% (with VPP-1, best MA yield was 39% at 340 °C), and the best PA yield was 5% at 360 °C (with VPP-1, it was 12% at 340 °C). Moreover, the formation of acids (acetic acid and acrylic acid) was remarkable with VPP-1 (higher overall yield close to 19% at 320 °C), whereas it was no

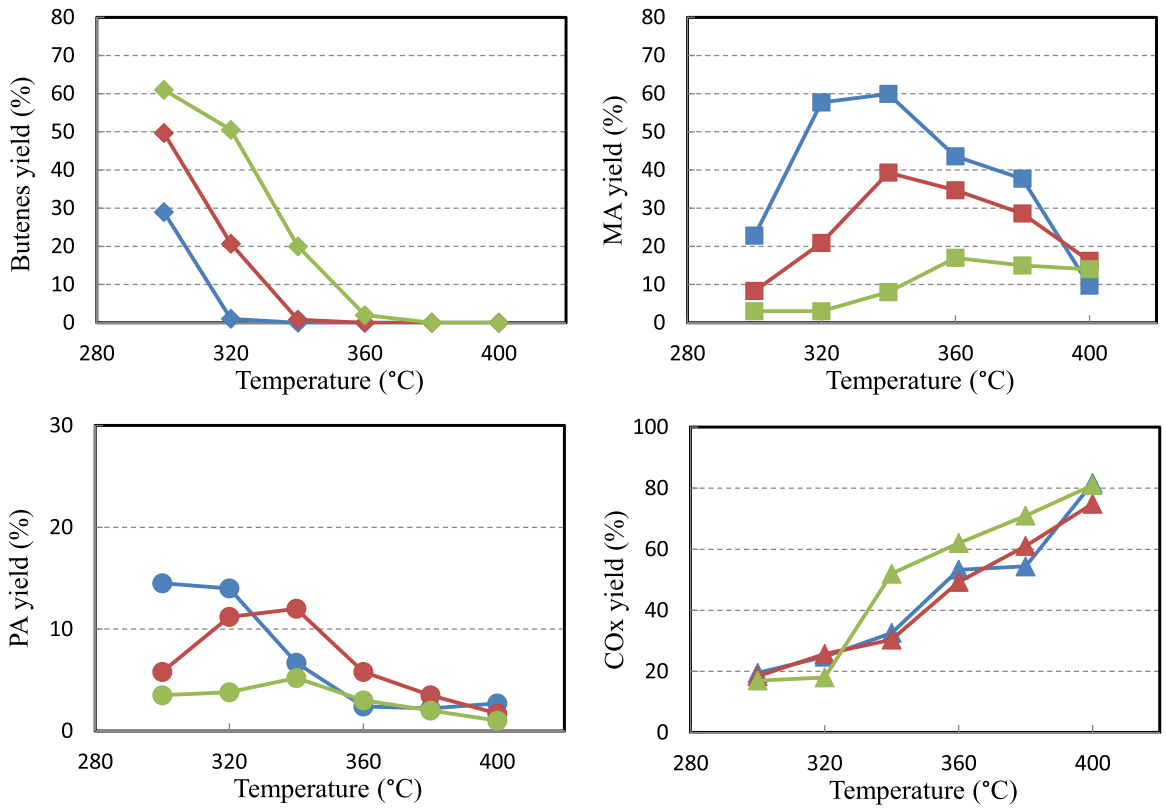

Fig. 3. Temperature effect on the catalytic behaviour of VPP-1 in 1-butanol oxidation. Feed 0.4 mol% 1-butanol in air (blue symbols and lines); 1.0 mol% 1-butanol in air (brown symbols and lines); 2.0 mol% 1-butanol in air (green symbols and lines). W/F 1.3 g_{cat} s/mL.

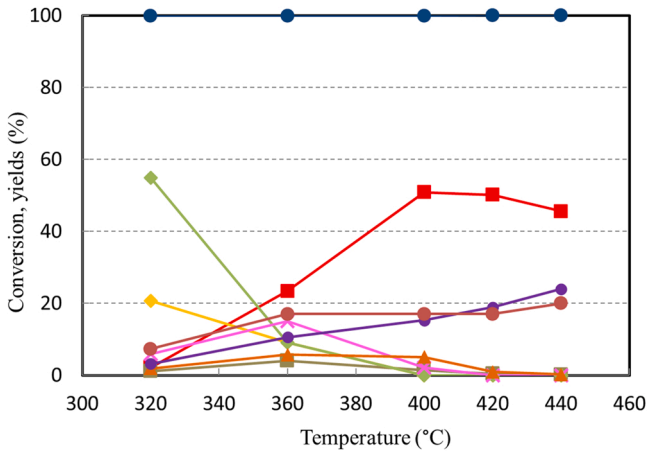

Fig. 4. Temperature effect on the catalytic behaviour of VPP-2 in 1-butanol oxidation. Feed 1.0 mol% 1-butanol in air. W/F 1.3 g_{cat}s/mL. Symbols as in Fig. 2.

higher than 5–6% (at 360–400 °C) with VPP-2.

The higher temperature needed with VPP-2 for the best MA yield can be explained by considering the above-described phenomenon of surface saturation, which is more evident with the low-surface-area VPP catalyst.

Moreover, in the case of VPP-1 a decline of both MA and PA yield was observed when the temperature was raised at above 340 °C, with an increase of both CO and CO_2 yield. Conversely, with VPP-2 the MA and PA decline occurred at above 400 °C and was less pronounced compared to that one observed with VPP-1. It is possible that the lower surface area of VPP-2 may limit consecutive combustion phenomena over both reactants and intermediates [45,46].

A similar behaviour, with three distinct zones of temperature each one with a prevailing class of products, i.e., alkenes in the low temperature range, partially oxidised products (MA, PA and acids) in the medium temperature range, and CO_x in the high temperature region, was also reported for the oxidation of *n*-butenes to MA, occurring via intermediate formation of butadiene [71,72]. Also in that case, the phenomenon was interpreted as being due to the interplay of both adsorption-desorption of reactants, intermediates and products, and availability of oxidising V sites; the latter was a function of the butene/O_2 inlet molar ratio.

Also with VPP-2, the best yield to MA declined considerably when the inlet concentration of 1-butanol was increased (Fig. 5).

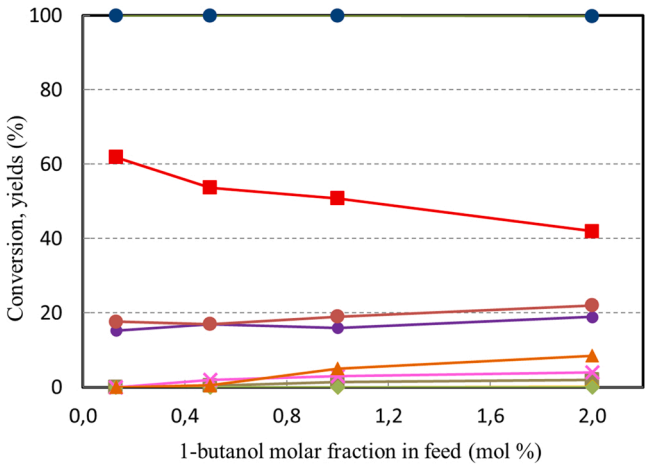

Fig. 5. Inlet molar fraction of 1-butanol effect on the catalytic behaviour of VPP-2 in 1-butanol oxidation. Feed: variable mol% 1-butanol in air. Temperature 400 °C; W/F 1.3 g_{cat} s/mL. Symbols as in Fig. 2.

3.3. Surface properties of vanadyl pyrophosphate catalysts, and relationship with catalytic performance

The role of surface characteristics on catalytic performance has been investigated by carrying out TPSR (Temperature Programmed Surface Reaction) experiments, using methanol as a model molecule. Methanol was chosen as a probe molecule because of the easier possibility to correlate surface features with the nature of products obtained; in fact, there is a wide literature available for the use of methanol as a probe molecule in the determination of catalysts surface features [73,74]. Conversely, there are very few information concerning the use of 1-butanol as a probe molecule [44]. The interaction of the two alcohols with the vanadyl pyrophosphate surface is expected to be the same in the two cases, occurring mainly via interaction of the -OH moiety with surface sites [44,73,74].

Firstly, methanol pulses were fed at 100 °C until saturation of the vanadyl pyrophosphate surface, then inert gas was flown on the sample while increasing the temperature, in order to react methanol and desorb the products from the surface; species desorbed were monitored by means of an online mass spectrometer.

Different reactions of methanol can take place on the catalytic surface, in function of the acid/base and redox sites present. Fig. 6 displays the reactions that may occur in the presence of acid/base sites (blue arrows) or redox sites (red arrows) [73,74]. The methanol pulses registered at the reactor outlet, after contact of methanol with the catalysts, are shown in Fig. S3.

In the case of VPP-2, very narrow pulses suggest negligible diffusional steps and limited chemical interaction between methanol and surface sites, whereas the opposite is true for VPP-1, since broader and less intense signals were shown. The comparison between the amount of methanol pulsed on catalysts and the amount of methanol not adsorbed (as calculated by the integration of pulses area) showed that with VPP-2 only the 2.0 ± 0.3% of the overall amount fed was adsorbed on catalyst surface, whereas in the case of VPP-1 the amount of the retained methanol was close to the 6.5 ± 0.7% of the amount fed. Therefore, the experimental value for VPP-1 was more than twice as much the value for VPP-2, so exceeding the ratio of surface areas for the two VPP samples (40 m^2/g for VPP-1 vs 20 m^2/g for VPP-2). This may point out that VPP-1 holds a more efficient interaction with methanol compared to VPP-2, leading to a greater amount of alcohol adsorbed, which was not only an effect of its greater value of surface area. A possible explanation may be the presence of a greater density of surface acid sites on VPP-1 surface (see later for the determination of the surface acidity).

After the adsorption of methanol, the nature and quantity of products desorbed during the increase of temperature under an inert flow were continuously monitored. In the case of VPP-2, which had previously adsorbed a smaller amount of methanol, the signals associated to products were less intense than in the case of VPP-1. The desorption of methanol for both catalysts took place between 100 and 200 °C, as shown in Fig. 7. In the same temperature range, also formaldehyde formed and desorbed, but the major amount of formaldehyde desorbed at 200–350 °C (Fig. 7 (right)).

CO formed in a very small amount, in the temperature range 250–350 °C for both catalysts. CO_2 also formed in very small amount, at above 300 °C. No methylformate, dimethylether and dimethoxymethane were observed; this suggests that no bimolecular reactions occurred, probably because of the very low concentration of methanol adsorbed.

The different intensity of the signals for the two catalysts may be once again attributed to the different surface area of the two samples, even though it is shown that the amount of methanol desorbed from VPP-1 was more than twice as much the amount desorbed from VPP-2 (Fig. 7 left).

The two samples were also characterised by means of ammonia-TPD (Fig. S4) to determine their acid properties. The desorption profiles for the two VPP catalysts were similar, with desorption occurring over the

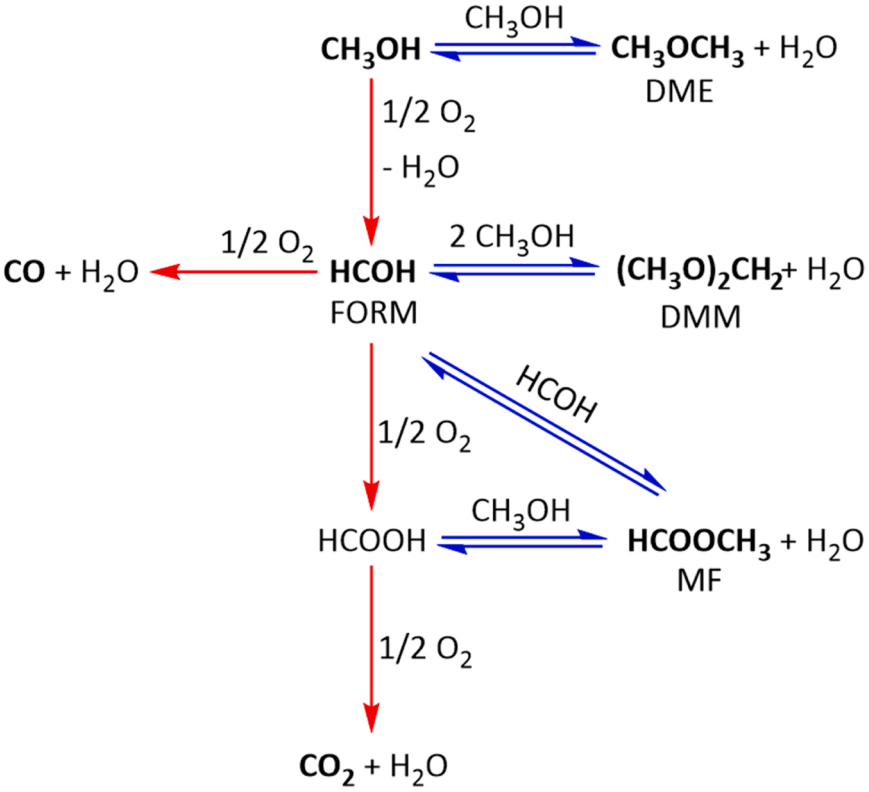

Fig. 6. Reaction scheme of methanol transformation over acid/base and redox sites. Blue arrows indicate reactions taking place on acid/base sites, red arrows on redox sites. FORM: formaldehyde; DME: dimethylether; DMM: dimethoxymethane; MF: methylformate.

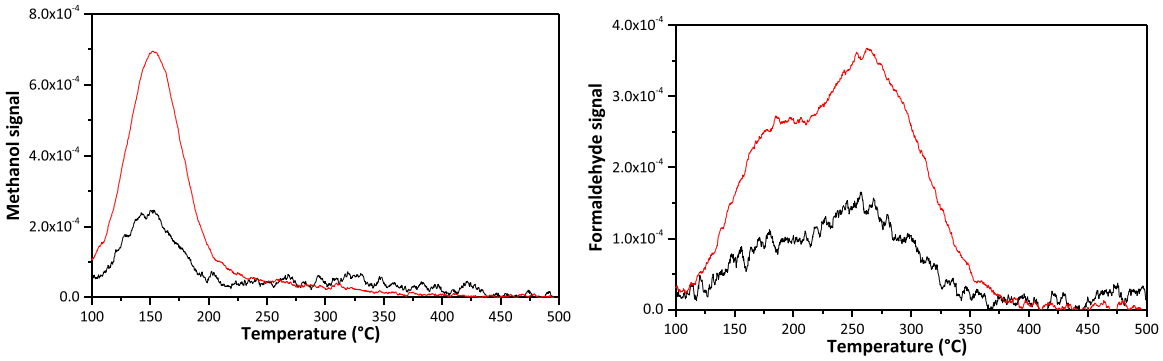

Fig. 7. MS signals of methanol (left) and formaldehyde (right) during methanol desorption with VPP-1 (red line) and VPP-2 (black line) catalysts. The VPD catalyst, characterised by very low surface area, did not provide reliable information; therefore, it has not been reported.

entire range of temperature investigated; a low-temperature desorption peak (150–250 °C) is attributable to weak acid sites, and the broad desorption occurring until 500–550 °C to medium strength sites. Instead, the high-temperature peak, occurring during the isothermal step but indeed starting already at 480–500 °C during the heating step, also derived from the oxidation of ammonia to N_2 and H_2O, with the concomitant reduction of V ions and loss of ionic oxygen. Not surprisingly, the overall amount of ammonia desorbed was greater for VPP-1 than for VPP-2, as expected because of the higher surface area of the former sample. However, the strong intensity of the low-temperature desorption peak (with an amount of ammonia desorbed with VPP-1 which was about 3 times as much the amount desorbed with VPP-2) points out for a density of surface sites in VPP-1 which is higher than that of VPP-2.

A higher density of acid sites, as shown by ammonia-TPD experiments, may be the reason for the greater yield of both light acids (deriving from cracking reactions) and PA observed with VPP-1, the formation of PA occurring via a Lewis-acid catalysed Diels-Alder addition between the intermediately formed butadiene and MA [44]. The same property may also be responsible for the enhanced dehydration of butanol to butenes, which occurs at lower temperature for VPP-1 (270–280 °C) compared to VPP-2 (ca. 320 °C). This also allows the conversion of butenes into MA to occur at lower temperature. On the other hand, acidity may be responsible for the rapid decline of MA selectivity observed with VPP-1 at temperature higher than 340 °C. Maleic anhydride, once formed, interacts more strongly with the catalyst surface, and may undergo an easier consecutive transformation into CO and CO_2. Conversely, with VPP-2 desorption may occur more easily (also because of the higher temperature needed), so saving MA from consecutive combustion. These data also agree with the stronger interaction between methanol and VPP-1 as recorded by means of methanol TPSR experiments.

3.4. The reactivity of VPP-1 in the dehydration of 1-butanol to butenes (in the absence of air)

The VPP-1 catalysts showed excellent performance in the dehydration of 1-butanol in the presence of oxygen; for example, high yield to butenes was shown at 200 °C (Fig. 2), with an overall yield to oxygenated compounds which was less than 5%.

The catalytic performance of VPP-1 in the absence of oxygen has also been investigated and the catalytic results, obtained by increasing the reaction temperature from 230 up to 340 °C, are shown in Fig. 8.

Again, complete 1-butanol conversion was achieved also ad low temperature. Interestingly, the reaction was totally selective to the formation of butenes with a carbon balance close to 100% until 320 °C, which however declined down to 90% at higher temperature. No oxidized compounds were found at 230 °C; at 260 °C, ca 2% yield to butyraldehyde was shown. This means that under these conditions the V

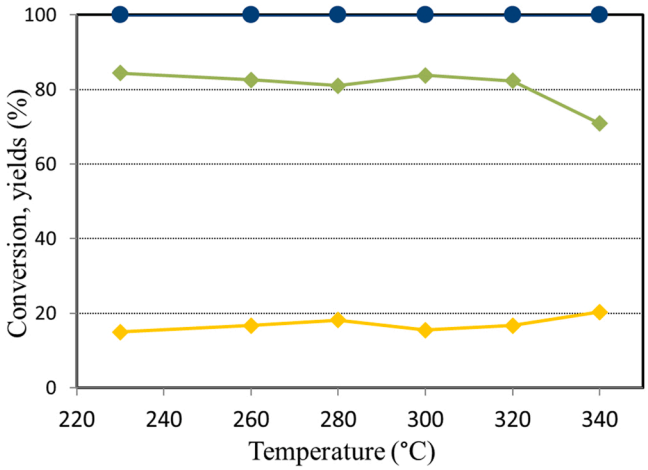

Fig. 8. Temperature effect on the catalytic behaviour of VPP-1 in 1-butanol dehydration. Feed 1.0 mol% 1-butanol in He. W/F 1.3 g_{cat}·s/mL. Symbols as in Fig. 2.

species (mainly present as V^{4+}) is not able to oxidise the organic substrate, and it needs the presence of gaseous O_2 to in-situ generate the active V^{5+} species required for the consecutive oxidation of butenes into MA. In fact, the used catalyst, characterised by means of Raman spectroscopy, was identical to the fresh one. Nevertheless, these results clearly confirmed the dehydrating ability of vanadyl pyrophosphate.

However, Fig. S5 shows that during prolonged reactivity experiments carried out at 260 °C, the catalyst underwent a slow, but non-negligible, deactivation. Conversely, when the reaction was carried out under the same conditions, but in the presence of air, no deactivation was observed (Fig. S6); on the other hand, in the latter case the selectivity to olefins declined, because of the formation of oxygenated by-products and carbon oxides with an overall selectivity close to 10%.

Thus, results obtained so far suggest that vanadyl pyrophosphate is a good catalyst for 1-butanol dehydration, but in the presence of air the selectivity to olefins is no higher than 90%, whereas under anaerobic conditions, selectivity is higher, but a slow deactivation takes place. The latter is attributable to the accumulation of char, the formation of which however is hindered when the reaction is carried out in the presence of air.

3.5. The reactivity of vanadium phosphate in the dehydration and oxidation of 1-butanol

We then tested the reactivity of VPD, in the presence and in the absence of oxygen; the catalyst was made of α_1-$VOPO_4$.

The results of experiments carried out without air in function of

temperature are shown in Fig. 9.

Products detected were butenes, butyraldehyde and *n*-butylether; C balance was better than 90% in the 260–300 °C T range, but it was between 70% and 90% outside of this interval. Almost total conversion was achieved at 280 °C, but higher temperatures led to a decline of conversion and of 2-butenes yield, suggesting a strong deactivation effect, which may be attributed to the deposition of carbonaceous residua over the catalytic surface. Best yields of butenes were obtained at 280 °C, with 70% of 2-butenes and 20% of 1-butene respectively.

The deactivation process was further investigated, by monitoring the catalytic behaviour during time-on-stream at 330 °C. The results, shown in Fig. S7, revealed a drop of conversion from 90% down to 32%; no variation in products distribution was observed. After the test, the spent catalyst underwent a regeneration treatment in air (see Experimental for detailed description of the regeneration procedure). The treated catalyst completely recovered its initial activity, but deactivation started again almost immediately.

The characterization of the catalyst after reaction at 330 °C showed that it had undergone modifications during reaction. Specifically, Raman spectra (Fig. S8) showed the accumulation of coke (bands at 1590–1600 and 1375–1380 cm^{-1} [75,76]), likely responsible for the remarkable deactivation phenomenon observed, and the presence of both α_1-$VOPO_4$ and $(VO)_2P_2O_7$. XRD pattern confirmed the presence of both compounds (Fig. S9). Vanadyl pyrophosphate likely formed by α_1-$VOPO_4$ reduction during reaction, because of the oxidative (however occurring in the absence of O_2) transformation of 1-butanol into butyraldehyde.

We then investigated the reactivity of the VPD catalyst in the presence of O_2; the catalytic performance in function of temperature is illustrated Fig. 10. It is shown that even in the presence of oxygen, the catalyst maintained its excellent performance in 1-butanol dehydration for temperatures comprised between 280 and 320 °C, with high selectivity and yield to butenes (the ratio between isomers being close to the thermodynamic value), with an excellent C balance and overall yield to oxygenates lower than 1.5%, and no *n*-butylether.

The catalytic behaviour was stable during a few hours' reaction time, as shown in Fig. S10; this is an important difference if compared to the behaviour in the absence of oxygen.

However, when the temperature was raised at above 360 °C, the catalyst started to behave similarly to the VPP, with transformation of alkenes and production of MA (but no PA), CO_x and light acids; C balance was close to 80% (Fig. 10).

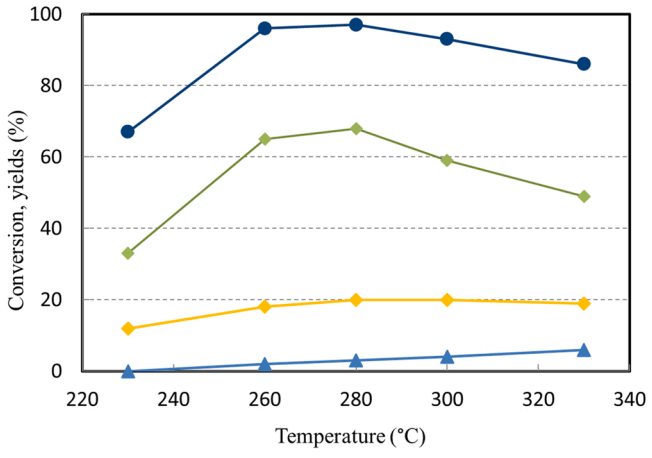

Fig. 9. Temperature effect on the catalytic behaviour of VPD in 1-butanol dehydration (each point was taken after one hour of reaction). Feed 1.0 mol % 1-butanol in He. W/F 1.3 g_{cat} s/mL. Symbols as in Fig. 2. Butyraldehyde (▲).

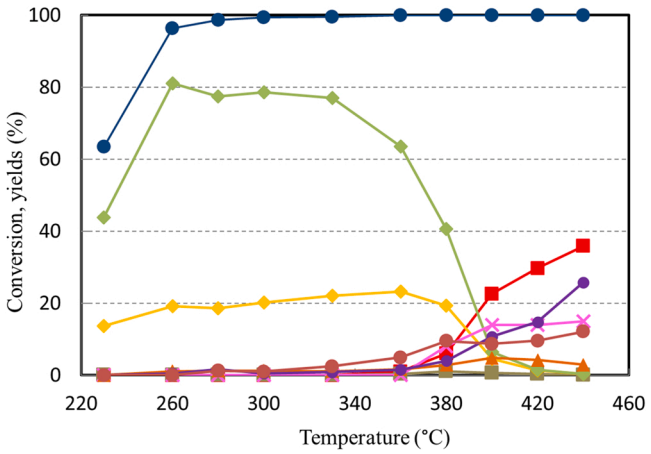

Fig. 10. Temperature effect on the catalytic behaviour of VPD in 1-butanol oxidation. Feed 1.0 mol% 1-butanol in air. W/F 1.3 g_{cat} s/mL. Symbols as in Fig. 2.

3.6. *The characterisation of used vanadium phosphate*

Ex-situ Raman spectra of the VPD catalyst after reaction at 440 °C in air are shown in Fig. S11, and reveal the presence of carbonaceous species (1600 and 1370 cm^{-1}), which is in agreement with the lack of carbon balance observed, and of α_1-$VOPO_4$, while the bands at 1185 and 1135 cm^{-1} are related to $(VO)_2P_2O_7$, which confirms the partial reduction of α_1-$VOPO_4$. The XRD pattern confirm indications from Raman spectra, however with the diffraction lines related to the vanadyl pyrophosphate as the prevailing ones (Fig. S12).

To confirm the hypothesized reduction of α_1-$VOPO_4$ during the oxidation of 1-butanol, an event which might be unexpected due to the presence of oxygen, we investigated the reduction of α_1-$VOPO_4$ into $(VO)_2P_2O_7$ by means of in-situ Raman experiments. The fresh catalyst was first calcined in order to transform $VOPO_4 2\,H_2O$ into α_1-$VOPO_4$. The experiment was then carried out by feeding 1.0 mol% 1-butanol in air, from 380 °C to 460 °C, thus simulating the same conditions of the laboratory plant (Fig. 11). The starting spectrum, before the reaction, showed bands at 1032, 928, 575, 540 and 288 cm^{-1} attributed to α_1-$VOPO_4$. After 240 min of reaction at 380 °C, the generation of two bands with a weak intensity at 1180 and 1130 cm^{-1} was observed, that could be correlated to the formation of $(VO)_2P_2O_7$. On increasing the temperature up to 400 °C, the bands attributable to the latter compound became clearly visible. A further increase of temperature and time led to the decrease of bands attributable to α_1-$VOPO_4$. At 460 °C, bands at 575, 540 and 288 cm^{-1} disappeared, while the intensity of the band at 1032 cm^{-1} was remarkably decreased, indicating the almost complete reduction of the V^{5+} phosphate.

These results explain the catalytic performance shown by the VPD catalyst in function of temperature; in fact, the in-situ development of the vanadyl pyrophosphate explains the progressive increase of the selectivity to MA. Reduction of the V^{5+} phosphate, despite the presence of O_2 in the gas-phase, suggests that under the conditions used the vanadyl pyrophosphate is the most stable crystalline structure. Under steady-state conditions, the latter acts as the basis for the V^{4+}/V^{5+} redox cycle leading to the generation of MA [46,48].

While cooling down the sample to room temperature in air, Raman spectra were recorded (Fig. S13); the interruption of 1-butanol feeding led to the growth of intensity of bands belonging to α_1-$VOPO_4$, with a concomitant decrease of the intensity of bands attributed to vanadyl pyrophosphate. This indicates that the reduction of $VOPO_4$ into $(VO)_2P_2O_7$ is, at least in part, a reversible process; after the reaction at 440 °C, part of the vanadyl pyrophosphate could be re-oxidised back into α_1-$VOPO_4$ when the temperature was decreased (while keeping the flow of air). This means that a dynamic phenomenon occurs with the

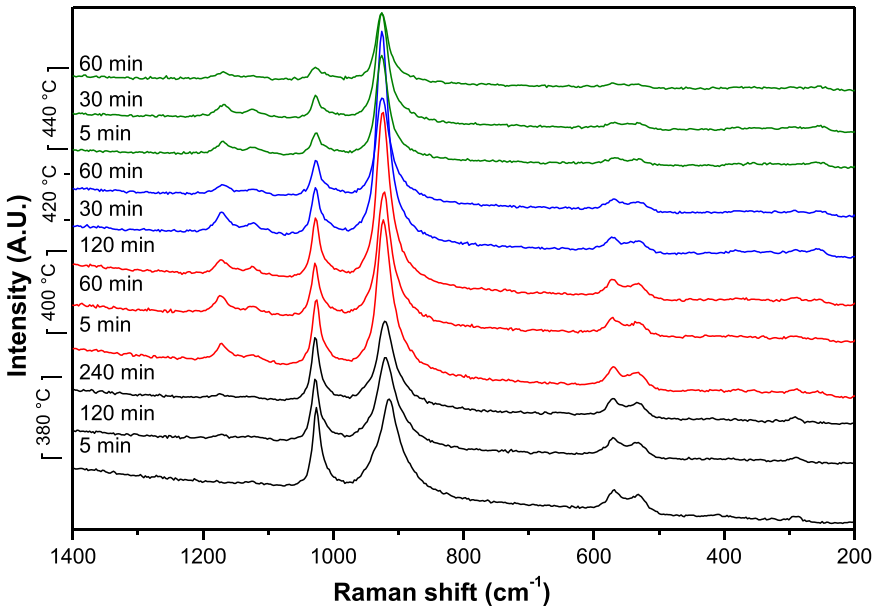

Fig. 11. In-situ Raman experiment of VPD catalyst while feeding 1.0 mol% 1-butanol in air at increasing temperatures.

interconversion of vanadyl pyrophosphate into vanadium phosphate, the prevailing compound (and the corresponding catalytic behavior) being a function of temperature and of gas-phase composition in the presence of the butanol/air mixture.

4. Conclusions

V/P/O-based catalysts show excellent performance in 1-butanol dehydration into butenes, but the catalytic performance is greatly affected by the characteristics of the catalyst and by reaction conditions. Vanadyl pyrophosphate, $(VO)_2P_2O_7$, the catalyst used in *n*-butane oxidation to maleic anhydride, shows very high yield to butenes at temperature lower than 240 °C in the presence of oxygen, whereas at higher temperatures it catalyzes the formation of maleic anhydride (60% yield) and phthalic anhydride (12% yield), but only when the molar fraction of 1-butanol in the inlet feed is very low, e.g., equal to 0.4 mol%. An increase of the 1-butanol concentration in the inlet feed leads to catalyst surface saturation effects which inhibit the consecutive oxidation steps leading to anhydrides formation. These phenomena are greatly affected by surface features, such as acidity; adsorption measurements carried out using methanol as the probe molecule confirmed the important role of adsorption and saturation phenomena. In the absence of oxygen, still the performance was excellent, with high yields to butenes, but the catalyst showed a slow deactivation due to the accumulation of tar, the latter being caused by catalyst surface acidity. The behavior of V^{5+} phosphate (α_1-$VOPO_4$) was different; the catalyst showed a remarkable deactivation in the absence of air during 1-butanol dehydration but showed a stable performance with very high yield to butenes at temperature lower than 340 °C, and in the presence of air. At higher temperature, the catalytic behavior of α_1-$VOPO_4$ became similar to that shown by vanadyl pyrophosphate, due to the in-situ transformation of the former into the latter compound.

Declaration of Competing Interest

The authors declare that they have no known competing financial interests or personal relationships that could have appeared to influence the work reported in this paper.

Data availability

The data that has been used is confidential.

Appendix A. Supporting information

Supplementary data associated with this article can be found in the online version at doi:10.1016/j.apcata.2023.119243.

References

[1] A. Chieregato, J. Velasquez Ochoa, F. Cavani, "Olefins from biomass", in: F. Cavani, S. Albonetti, F. Basile, A. Gandini (Eds.), Chemicals and Fuels from Bio-Based Build. Blocks, Wiley-VCH Verlag, Weinheim, Germany, 2016, pp. 3–33.
[2] V. Zacharopoulou, A. Lemonidou, Catalysts 8 (2017) 2–19.
[3] S. Shylesh, A.A. Gokhale, C.R. Ho, A.T. Bell, Acc. Chem. Res. 50 (2017) 2589–2597.
[4] D. Sun, S. Sato, W. Ueda, A. Primo, H. Garcia, A. Corma, Green. Chem. 18 (2016) 2579–2597.
[5] M. Brodin, M. Vallejos, M.T. Opedal, M.C. Area, G. Chinga-Carrasco, J. Clean. Prod. 162 (2017) 646–664.
[6] B. Bharathiraja, J. Jayamuthunagai, T. Sudharsanaa, A. Bharghavi, R. Praveenkumar, M. Chakravarthy, D. Yuvaraj, Renew. Sustain. Energy Rev. 68 (2017) 788–807.
[7] P. Haro, P. Ollero, F. Trippe, Fuel Process. Technol. 114 (2013) 35–48.
[8] I.S. Yakovleva, S.P. Banzaraktsaeva, E.V. Ovchinnikova, V.A. Chumachenko, L. A. Isupova, Catal. Ind. 8 (2016) 152–167.
[9] A. Maneffa, P. Priecel, J.A. Lopez-Sanchez, ChemSusChem 9 (2016) 2736–2748.
[10] M. Zhang, Y. Yu, Ind. Eng. Chem. Res. 52 (2013) 9505–9514.
[11] D. Fan, D.J. Dai, H.S. Wu, Materials 6 (2013) 101–115.
[12] B. Chen, J. Lu, L. Wu, Z. Chao, Cuihua Xuebao/Chin. J. Catal. 37 (2016) 1941–1948.
[13] I. Rossetti, M. Compagnoni, E. Finocchio, G. Ramis, A. Di Michele, Y. Millot, S. Dzwigaj, Appl. Catal. B Environ. 210 (2017) 407–420.
[14] R. Feng, X. Hu, X. Yan, Z. Yan, M.J. Rood, Micro Mesoporous Mater. 241 (2017) 89–97.
[15] T.T.N. Nguyen, V. Ruaux, L. Massin, C. Lorentz, P. Afanasiev, F. Maugé, V. Bellière-Baca, P. Rey, J.M.M. Millet, Appl. Catal. B Environ. 166 (167) (2015) 432–444.
[16] T.T.N. Nguyen, V. Ruaux, F. Maugé, V. Bellière-Baca, P. Rey, J.M.M. Millet, Appl. Catal. A Gen. 504 (2015) 4–10.
[17] T.T.N. Nguyen, V. Bellière-Baca, P. Rey, J.M.M. Millet, Catal. Sci. Technol. 5 (2015) 3576–3584.
[18] D. Gunst, K. Alexopoulos, K. Van Der Borght, M. John, V. Galvita, M.F. Reyniers, A. Verberckmoes, Appl. Catal. A 539 (2017) 1–12.
[19] D. Gunst, M. Sabbe, M.-F. Reyniers, A. Verberckmoes, Appl. Catal. A 582 (2019), 117101.
[20] A. de Reviere, D. Gunst, M. Sabbe, A. Verberckmoes, J. Ind. Eng. Chem. 89 (2020) 257–272.
[21] A. de Reviere, D. Gunst, M.K. Sabbe, M.-F. Reyniers, A. Verberckmoes, Catal. Sci. Technol. 11 (2021) 2540–2559.
[23] M. John, K. Alexopoulos, M.F. Reyniers, G.B. Marin, Catal. Sci. Technol. 7 (2017) 2978–2997.

[24] M. John, K. Alexopoulos, M.F. Reyniers, G.B. Marin, A.C.S. Catal 6 (2016) 4081–4094.
[25] M. John, K. Alexopoulos, M.F. Reyniers, G.B. Marin, Catal. Sci. Technol. 7 (2017) 1055–1072.
[26] M. John, K. Alexopoulos, M.F. Reyniers, G.B. Marin, J. Catal 330 (2015) 28–45.
[27] D. Zhang, S.A.I. Barri, D. Chadwick, Appl. Catal. A Gen. 403 (2011) 1–11.
[28] S. Zhao, W. Yang, K. Duk Kim, L. Wang, Z. Wang, R. Ryoo, J. Huang, J. Phys. Chem. C. 125 (2021) 11665–11676.
[29] A. Micek-Ilnicka, N. Ogrodowicz, U. Filek, A. Kusior, Catal. Today 380 (2021) 84–92.
[30] T. Kella, A. Anandan Vennathan, S. Dutta, S. Sankar Mal, D. Shee, Mol. Catal. 516 (2021), 111975.
[31] E. Hong, H.-I. Sim, C.-H. Shin, Chem. Eng. J. 292 (2016) 156–162.
[32] J. Wu, H.-J. Liu, X. Yan, Y.-J. Zhou, Z.-N. Lin, S. Mi, K.-K. Cheng, J.-A. Zhang, Catalysts 9 (2019) 93–106.
[33] J. Ballesteros-Soberanas, L.D. Ellis, J.W. Medlin, A.C.S. Catal 9 (2019) 7808–7816.
[34] C. Lang, J. Schnee, B.J. Takam Mba, F. Devred, E.M. Gaigneaux, Catal. Sci. Technol. 10 (2020) 6244–6256.
[35] F. Li, X. Dai, X. Lu, C. Wang, W. Qi, Catal. Sci. Technol. 11 (2021) 4500–4508.
[36] J. Soto, J.M. Rosas, J.C. Otero, J. Rodríguez-Mirasol, T. Cordero, J. Phys. Chem. C. 122 (2018) 16772–16778.
[37] D. Shi, H. Wang, L. Kovarik, F. Gao, C. Wan, J. Zhi Hu, Y. Wang, J. Catal. 363 (2018) 1–8.
[38] C.D. Baertsch, K.T. Komala, Y.H. Chua, E. Iglesia, J. Catal. 205 (2002) 44–57.
[39] J. Macht, C.D. Baertsch, M. May-Lozano, S.L. Soled, Y. Wang, E. Iglesia, J. Catal. 227 (2004) 479–491.
[40] E. Hong, H.I. Sim, C.H. Shin, Chem. Eng. J. 292 (2016) 156–162.
[41] Z. Buniazet, A. Cabiac, S. Maury, D. Bianchi, S. Loridant, Appl. Catal. B 243 (2019) 594–603.
[42] S. Van Daele, D. Minoux, N. Nesterenko, S. Maury, V. Coupard, V. Valtchev, A. Travert, J.-P. Gilson, Appl. Catal. B 284 (2021), 119699.
[43] N. Ballarini, F. Cavani, C. Cortelli, S. Ligi, F. Pierelli, F. Trifirò, C. Fumagalli, G. Mazzoni, T. Monti, Top. Catal. 38 (2006) 147–156.
[44] G. Pavarelli, J. Velasquez Ochoa, A. Caldarelli, F. Puzzo, F. Cavani, J.-L. Dubois, ChemSusChem 8 (2015) 2250–2259.
[45] N.F. Dummer, J.K. Bartley, G.J. Hutchings, Adv. Catal. 54 (2011) 189–247.
[46] A. Caldarelli, M.A. Bañares, C. Cortelli, S. Luciani, F. Cavani, Catal. Sci. Technol. 4 (2014) 419–427.
[47] N.P. Rajan, G.S. Rao, B. Putrakumar, K.V.R. Chary, R.S.C. Adv 4 (2014) 53419–53428.
[48] F. Cavani, S. Luciani, E.D. Esposti, C. Cortelli, R. Leanza, Chem. Eur. J. 16 (2010) 1646–1655.
[49] A. Chieregato, J.M. López Nieto, F. Cavani, Coord. Chem. Rev. 301 302 (2015) 3–23.
[50] F. Cavani, J.H. Teles, ChemSusChem 2 (2009) 508–534.
[51] G.J. Hutchings, J. Mater. Chem. 14 (2004) 3385.
[52] F. Cavani, A. Colombo, F. Giuntoli, E. Gobbi, F. Trifirò, P. Vazquez, Catal. Today 32 (1996) 125–132.
[53] D.J. Upadhyaya, S.D. Samant, Catal. Today 208 (2013) 60–65.
[54] N. Pethan Rajan, G.S. Rao, V. Pavankumar, K.V.R. Chary, Catal. Sci. Technol. 4 (2014) 81–92.
[55] F. Wang, J.-L. Dubois, W. Ueda, J. Catal. 268 (2009) 260–267.
[56] F. Wang, J.-L. Dubois, W. Ueda, Appl. Catal. A Gen. 376 (2010) 25–32.
[57] A. Martin, U. Bentrup, B. Lücke, A. Brückner, Chem. Commun. (1999) 1169–1170.
[58] G. Busca, G. Centi, F. Trifirò, V. Lorenzelli, J. Phys. Chem. 90 (1986) 1337–1344.
[59] I. Sádaba, S. Lima, A.A. Valente, M. López Granados, Carbohydr. Res. 346 (2011) 2785–2791.
[60] T. Tabanelli, M. Mari, F. Folco, F. Tanganelli, F. Puzzo, L. Setti, F. Cavani, Appl. Catal. A 619 (2021), 118139.
[61] M.T. Nguyen Dinh, T.L. Nguyen, M.D. Phan, L. Nguyen Dinh, Q.D. Truong, E. Bordes-Richard, J. Catal. 377 (2019) 638–651.
[62] C. Schulz, S.C. Roy, K. Wittich, R. Naumann d'Alnoncourt, S. Linke, V.E. Strempel, B. Frank, R. Glaum, F. Rosowski, Catal. Today 333 (2019) 113–119.
[63] M. Müller, M. Kutscherauer, S. Bocklein, G.D. Wehinger, T. Turek, G. Mestl, Catal. Today 387 (2022) 82–106.
[64] C. Schulz, F. Pohl, M. Driess, R. Glaum, F. Rosowski, B. Frank, Ind. Eng. Chem. Res. 58 (2019) 2492–2502.
[65] W. Li, Y. Xiao, S. Guo, L. Jia, H. Guo, D. Li, Fuel 333 (2023), 126214.
[66] S. Badehbakhsh, N. Saadatkhah, M. Jaber Darabi Mahboub, O. Guerrero-Perez, G. S. Patience, Catal. Today 407 (2023) 301–311.
[67] N.F. Dummer, W. Weng, C.J.C. Kiely, A.F. Carley, J.K. Bartley, C.J.C. Kiely, G. J. Hutchings, Appl. Catal. A 376 (2010) 4755.
[68] F. Ben Abdelouahab, R. Oliver, N. Guilhaume, F. Lefebvre, J.C. Volta, J. Catal 134 (1992) 151–167.
[69] J. Happel, M.A. Hnatow, R. Mezaki, J. Chem. Eng. Data 16 (1971) 206–209.
[70] G. Bignardi, F. Cavani, C. Cortelli, T. De Lucia, F. Pierelli, F. Trifirò, G. Mazzoni, C. Fumagalli, T. Monti, J. Mol. Catal. A Chem. 244 (2006) 244–251.
[71] F. Cavani, G. Centi, I. Manenti, Ind. Eng. Chem. Prod. Res. Dev. 29 (1983) 565–570.
[72] F. Cavani, G. Centl, F. Trifirò, Ind. Eng. Chem. Prod. Res. Dev. 22 (1983) 570–577.
[73] J.M. Tatibouët, Appl. Catal. A Gen. 148 (1997) 213–252.
[74] G. Busca, Catal. Today 27 (1996) 457–496.
[75] R. Vidano, D.B. Fischbach, J. Am. Ceram. Soc. 61 (1978) 13–17.
[76] K. Angoni, J. Mater. Sci. 33 (1998) 3693–3698.